Journal of Applied Geophysics 105 (2014) 59–66

Contents lists available at ScienceDirect

Journal of Applied Geophysics

journal homepage: www.elsevier.com/locate/jappgeo

Hydrocarbon detection using adaptively selected spectrum attenuation

Lingling Wang [a,b,*], Jinghuai Gao [b,c], Zongben Xu [a], Bing Weng [d], Xiudi Jiang [d]

[a] School of Mathematics and Statistics, Xi'an Jiaotong University, Xi'an, Shaanxi 710049, China
[b] National Engineering Laboratory for Offshore Oil Exploration, Xi'an, Shaanxi 710049, China
[c] School of Electronic and Information Engineering, Xi'an Jiaotong University, Xi'an, Shaanxi 710049, China
[d] Research Center of CNOOC, Beijing 100027, China

ARTICLE INFO

Article history:
Received 6 July 2013
Accepted 8 March 2014
Available online 14 March 2014

Keywords:
Spectrum attenuation
Hydrocarbon detection
Short-Time Fourier Transform
Attenuation selection
Edge-preserving smoothing

ABSTRACT

Hydrocarbon reservoir usually shows the characteristics of low frequency amplifying and high frequency attenuating, which has been used as hydrocarbon indicator. However, reflection interference may also cause these phenomenons. In this paper, we propose an adaptively selected spectrum attenuation method to reduce the impact of the reflection interference in hydrocarbon detection. We first evaluate spectrum attenuation of seismic data by calculating the ratio of high frequency to low frequency components for each trace in the time-frequency domain. Notice that high frequency components are not really attenuated by interference as they appear, they can be recovered later, so we use an edge-preserving smoothing (EPS) method to smooth the equivalent local peak frequencies (ELPFs) located at the local peaks of seismic envelope to measure the attenuation trend of a seismic trace, and choose the spectrum attenuation whose high frequency components are really attenuated to locate the hydrocarbon. A real seismic data example demonstrates that the spectrum attenuation calculated by the ratio can avoid the impact of strong reflection, and the selected spectrum attenuation can reduce the effect of interference, which makes it more reliable in locating hydrocarbons than use the spectrum attenuation directly.

1. Introduction

Since the inception of bright spot technology in the 1960s, low-frequency shadows beneath amplitude anomalies have been used as a substantiating hydrocarbon indicator (HI). At the 1996 SEG/EAGE Summer Research Workshop, Dan Ebrom summarized at least 10 mechanisms that can explain these low-frequency shadows (Ebrom, 2004). Following that, Castagna et al. (2003) use instantaneous spectral analysis (ISA) based on Mallat's matching pursuit decomposition to directly detect hydrocarbons for gas reservoirs from high frequency attenuation anomalies, and/or low frequency shadows. Sa et al. (2004) and Hu et al. (2005) demonstrate that hydrocarbon reservoir shows low frequency resonating (LFR) and high frequency attenuating (HFA) through laboratory testing, numerical simulation and petrological analysis based on multi-phase theory and double-phase theory respectively. This discovery therefore further explains the low-frequency shadows and provides some new methods to directly detect oil and gas using seismic information (Hu et al., 2005, 2009; Sa et al., 2004). Chen and Gao (2007) proposed to detect hydrocarbons by using the difference between high and low frequency components based on their modified best matching seismic wavelets (MBMSW). Jiang et al. (2010) combined the high frequency attenuation gradient and low frequency energy information using MBMSW to detect hydrocarbon. Zhou et al. (2010) decomposed seismic data trace by trace into a set of Ricker wavelets with different dominant frequencies using wavelet transform (WT), and for each trace calculated the difference of two amplitude spectrums, one of which is computed by adding up the WT amplitude spectrums inside a window above the target layer under investigation and the other from a window below the target layer. The two amplitude spectrums are normalized before computing their difference. Then the locations with negative values at low frequency and positive values at high frequency may indicate being hydrocarbon-bearing (Zhou et al., 2010).

However, if the layers are thin enough, reflections at the boundaries will interfere with each other, and their superposition may produce a 'fat' compound waveform which has much lower dominant frequency. As a result, the high frequency components appear to be attenuated and the low frequency components may be increased for the seismic trace at the time window, which will mislead us in hydrocarbon detection. In reality, when the layers are thick enough at a later time, no

* Corresponding author at: School of Mathematics and Statistics, Xi'an Jiaotong University, No. 28, Xianning West Road, Xi'an, Shaanxi, 710049, China. Tel: +86 29 82665060.
E-mail addresses: w.linglingx@gmail.com (L. Wang), jhgao@mail.xjtu.edu.cn (J. Gao), zbxu@mail.xjtu.edu.cn (Z. Xu).

http://dx.doi.org/10.1016/j.jappgeo.2014.03.005
0926-9851/

interference will present, the reflected waves as well as these frequency components will recover. Taking advantage of this, we propose an adaptively selected spectrum attenuation method to reduce the impact of interference in hydrocarbon detection. We first transform seismic data into time–frequency domain using Short-Time Fourier Transform (STFT) trace by trace, then derive spectrum attenuation for each trace by calculating the ratio of high frequency to low frequency component. Then we use an edge-preserving smoothing (EPS) method to smooth the equivalent local peak frequencies (ELPFs) located at the local peaks of seismic envelope to find the attenuation trend of the high frequency components. Finally, hydrocarbons are detected by choosing the spectrum attenuation whose high frequency components are really attenuated.

2. Theory

2.1. Short-Time Fourier Transform

Following Mallat (2003), we introduce windowed Fourier atom which is constructed by a real and symmetric window $g(t) = g(-t)$ translated by u in time and by ξ in frequency:

$$g_{u,\xi}(t) = g(t-u)\exp(i\xi t). \quad (1)$$

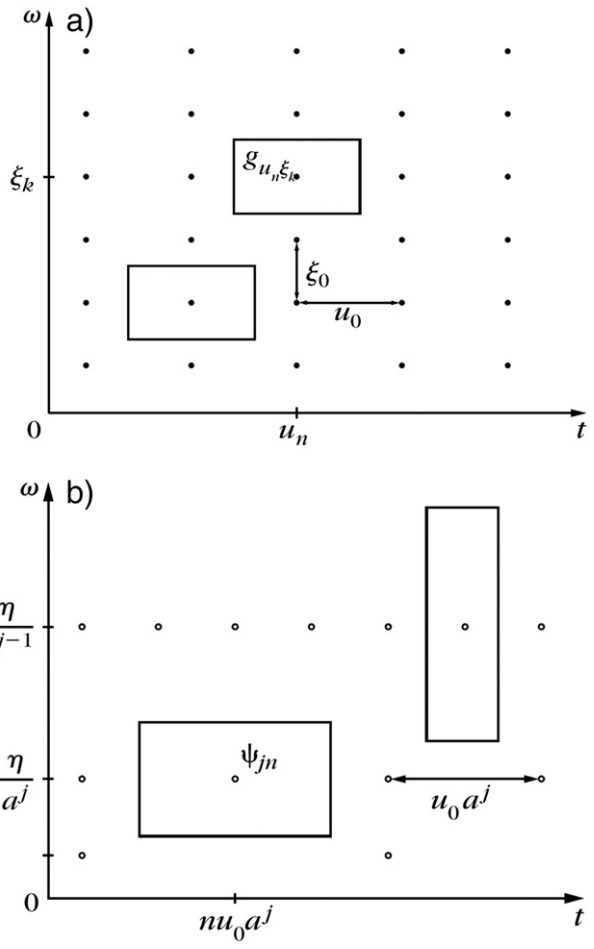

Fig. 1. Heisenberg time–frequency boxes of (a) Short-Time Fourier frame covering the time–frequency plane with a regular grid of Short-Time Fourier atoms, translated by $u_n = nu_0$ in time and by $\xi_k = k\xi_0$ in frequency, and (b) wavelet frame scaled by $s = a^j$ has a time and frequency width proportional to a^j and a^{-j} respectively. Mallat (2003).

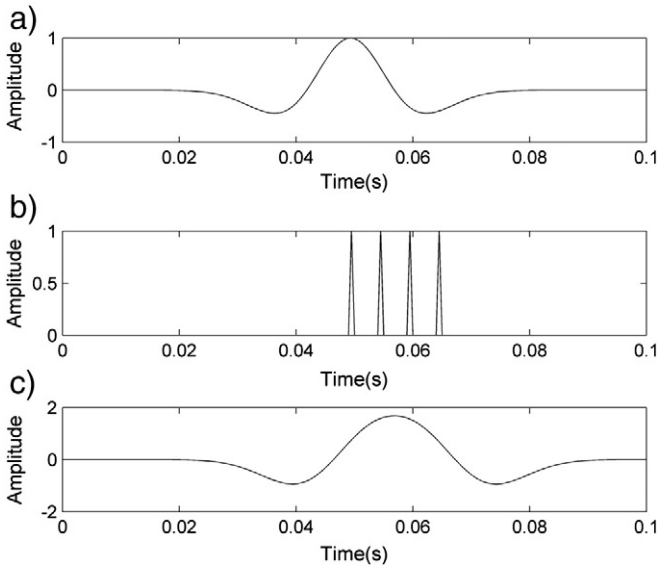

Fig. 2. Thin bed model example. (a) 30 Hz Ricker wavelet; (b) thin bed model with four reflectivity coefficients which have the same magnitude and sign; (c) synthetic seismic trace generated by convolving (a) with (b).

It is normalized such that $\|g\| = 1$, thus $\|g_{u,\xi}\| = 1$ for any $(u, \xi) \in R^2$. The resulting Short-Time Fourier Transform (STFT) of $s \in L^2(R)$ is

$$S(u,\xi) = \left\langle s, g_{u,\xi} \right\rangle = \int_{-\infty}^{\infty} s(t)g(t-u)\exp(-i\xi t)dt \quad (2)$$

where u is the location of the window center, $\xi = 2\pi f$, the multiplication by $g(t-u)$ localizes the Fourier integral in the neighborhood of $t = u$.

If we discrete the time and frequency parameters (u, ξ) over a rectangular grid with time and frequency intervals of size u_0 and ξ_0, we can get the Short-Time Fourier frame $g_{n,k}(t) = g(t - nu_0)\exp(ik\xi_0 t)$, and the corresponding Heisenberg boxes representing the energy spread of Short-Time Fourier frame (Mallat, 2003) are illustrated in Fig. 1a. From this figure, we can see that the frequency of STFT is regular, so the low frequency and high frequency components are comparable. And if ξ_0 is sufficiently small, the frequency will be densely sampled, which will be more accurate for measuring the attenuation trend.

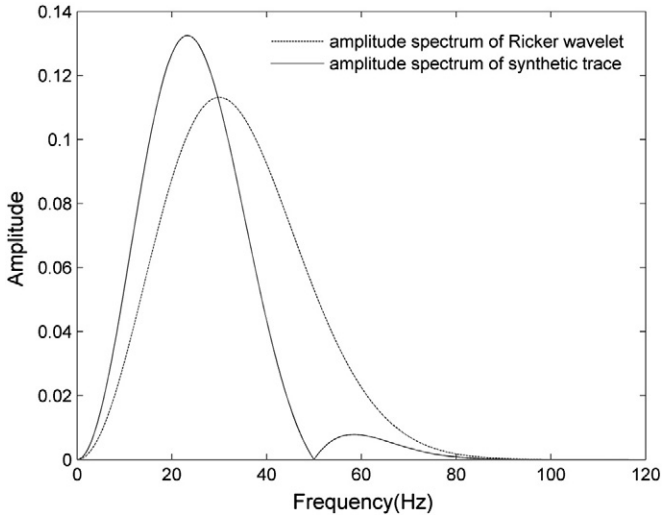

Fig. 3. Energy normalized amplitude spectrum of the 30 Hz Ricker wavelet in Fig. 2a (dotted line) and the synthetic seismic trace in Fig. 2c (solid line).

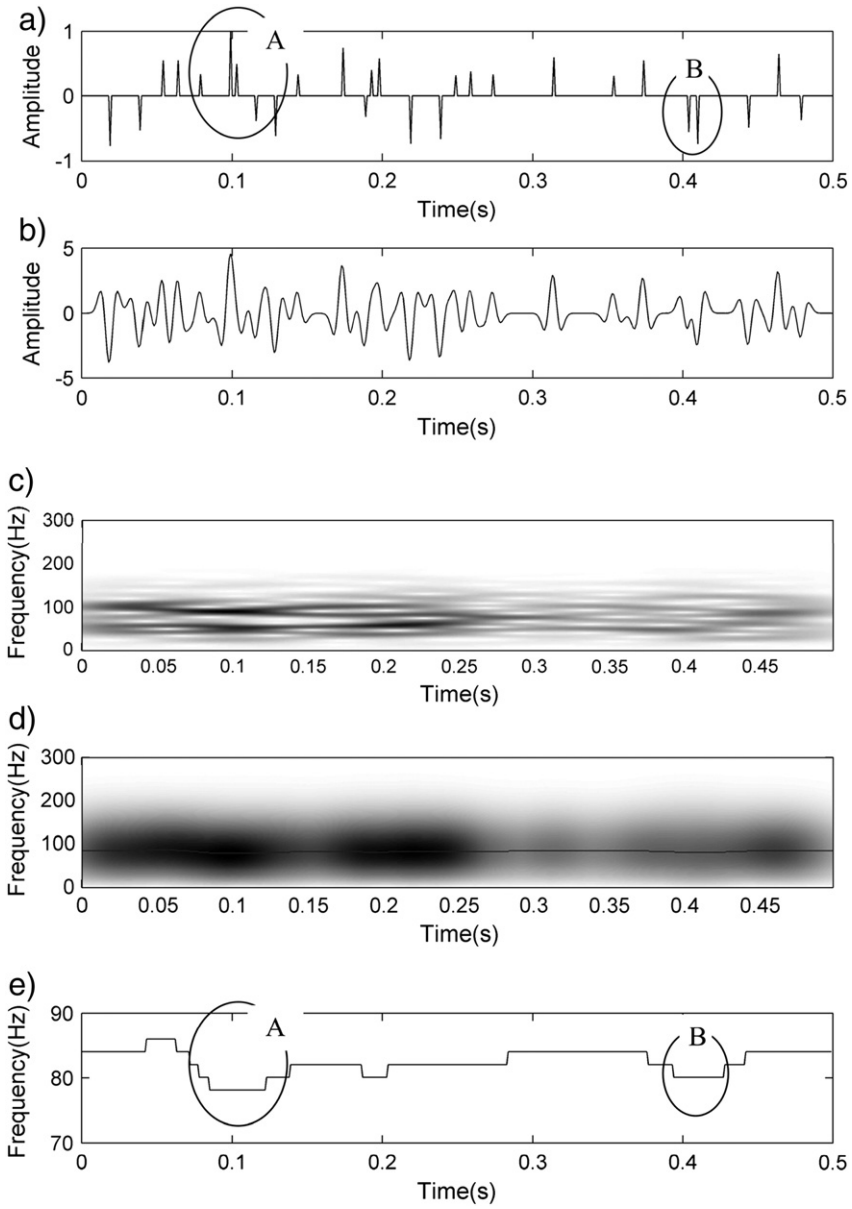

Fig. 4. Interference effect illustrated by synthetic seismic trace without attenuation. (a) the reflectivity; (b) the synthetic seismic trace without attenuation; (c) the STFT amplitude spectrum of (b); (d) the smoothed STFT amplitude spectrum corresponding to (c) and its equivalent local peak frequencies (solid line); (e) zoom in the equivalent local peak frequencies in (d). Ellipses A and B show the sections influenced by interference.

While for the wavelet frame defined by $\psi_{j,n}(t) = \frac{1}{\sqrt{a^j}}\psi\left(\frac{t-nu_0a^j}{a^j}\right)$ as illustrated in Fig. 1b, the frequency is not regular, which makes it not suitable for measuring attenuation trend or selecting spectrum attenuation. So we choose STFT as an analysis tool in this paper.

2.2. Spectrum attenuation based on STFT

It is usually observed that the seismic waves will be abnormally attenuated in high frequency and amplified in low-frequency travelling through the gas-filled reservoirs (Biot, 1956; Castagna et al., 2003; Goloshubin and Korneev, 2000; Hu et al., 2005; Klimentos, 1995; Korneev et al., 2004; Mitchell et al., 1996; Palmer and Traviolia, 1980; Sa et al., 2004). Therefore, in this paper, we use spectrum attenuation defined as the ratio of two spectrums, one is computed from low frequency components and the other from high frequency components, to locate the hydrocarbon.

Let $s(x,t)$ be a 2D seismic profile, where x is the position of the detector, t is the time. $\{S(f, x, t), 0 < f < F\}$ denotes the STFT amplitude spectrum of $s(x,t)$, where f is the frequency, F is the cut-off frequency. We calculate the amplitude spectrum of high frequency by averaging the amplitude spectrums in the high frequency band $\{f_{H_1}, f_{H_2} \cdots f_{H_{N1}}\}$ as

$$S\left(\overline{f}_H, x, t\right) = \sum_{i=1}^{N1} S\left(f_{H_i}, x, t\right)/N1 \tag{3}$$

where $N1$ is the number of high frequency components. Similarly, we calculate the amplitude spectrum of low frequency by averaging the amplitude spectrums in the low frequency band $\left\{f_{L_1}, f_{L_2} \cdots f_{L_{N2}}\right\}$ as

$$S\left(\overline{f}_L, x, t\right) = \sum_{i=1}^{N2} S\left(f_{L_i}, x, t\right)/N2 \tag{4}$$

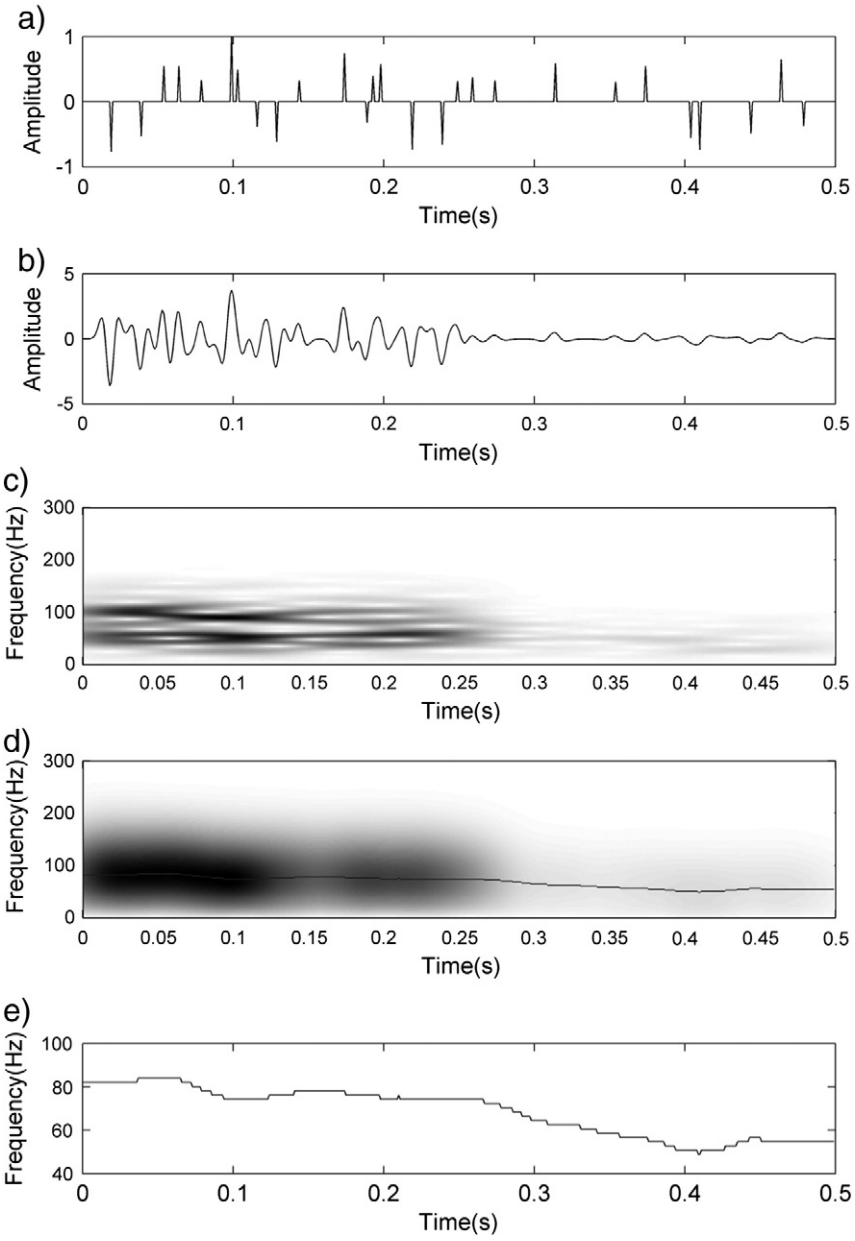

Fig. 5. Interference effect illustrated by synthetic seismic trace with attenuation. (a) The reflectivity; (b) the synthetic seismic trace with attenuation (Q = 100 for t = 0–0.25 s, Q = 80 for t = 0.25–0.5 s); (c) the STFT amplitude spectrum of (b); (d) the smoothed STFT amplitude spectrum corresponding to (c) and its equivalent local peak frequencies (solid line); (e) zoom in the equivalent local peak frequencies in (d).

where *N*2 is the number of low frequency components. Then we express the spectrum attenuation of the seismic profile as

$$Q(x,t) = 1 - S\left(\overline{f}_H, x, t\right) / S\left(\overline{f}_L, x, t\right). \quad (5)$$

Here, we subtract the ratio from 1 to highlight strong spectrum attenuation as the hydrocarbon indicator.

2.3. Spectrum attenuation selection

The interference of seismic waves may also cause the attenuation of high frequency energy and the increase of the low frequency energy, which can produce strong spectrum attenuation in Eq. (5). As a result, it may mislead the detection of hydrocarbons. To demonstrate this, we generate a synthetic seismic trace (Fig. 2c) by convolving a 30 Hz Ricker wavelet (Fig. 2a) with a thin bed reflectivity (Fig. 2b). Fig. 3 compares the energy normalized amplitude spectrum of the source wavelet in Fig. 2a with that of the synthetic seismic trace in Fig. 2c. We can see that, the interference of seismic waves that compose the synthetic trace causes high frequency energy attenuation and low frequency energy increase relatively.

In this section, we propose a spectrum attenuation selection method to reduce the effect of interference that we observed in the previous example. As mentioned above, these high frequency components are not really attenuated by interference as they appear, low frequency components are not increased either. So, in this paper we propose an equivalent local peak frequency based method to select the spectrum attenuation. In theory, seismic attenuation always causes the peak frequency of the seismic wavelet to decrease with travel time (Zhang and Ulrych, 2002). We transform the seismic trace into the STFT domain, and use a moving average smoothing method to smooth the

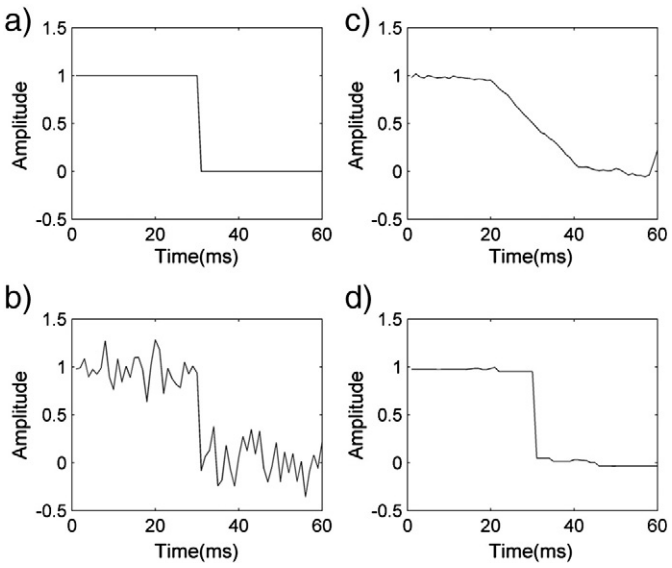

Fig. 6. 1D EPS filter. (a) Step function without noise; (b) step function with noise added; (c) result after moving average smoothing method; (d) result after 1D EPS smoothing. Both smoothing methods use a 21-point operator.

amplitude spectrum of each windowed trace segment in the STFT domain. Then we approximately obtain the amplitude spectrum of the wavelet for each segment, which is determined by both the source wavelet and local attenuation effects. We call this wavelet the equivalent wavelet of that segment. Subsequently we take the peak frequency of each equivalent wavelet as the equivalent local peak frequency (ELPF) of the seismic trace at each sample. We use these ELPFs extracted from the smoothed STFT amplitude spectrum to measure the attenuation trend of the trace. If the ELPF is recovered in a later time window, we will classify the strong spectrum attenuation of this seismic segment as having resulted from seismic interference, which will be removed from the final hydrocarbon indicator as illustrated in Fig. 4, where Fig. 4e shows the ELPFs of the synthetic seismic trace without attenuation in Fig. 4b. From Fig. 4e we can see that, although the ELPFs decrease in some sections due to the interference of seismic waves, as marked by ellipses A and B, they are not really decreased, they recover well in a later time window. In contrast, Fig. 5e shows the ELPFs of the synthetic seismic trace with attenuation in Fig. 5b. From this figure we can see that the ELPFs are really decreased due to attenuation.

In practice, it is often hard to exactly extract an equivalent wavelet from the amplitude spectrum of each segment by the smoothing method due to the influence of interference, noises etc. As a result, the ELPFs derived from these equivalent wavelets are also disturbed. In this paper, we apply edge-preserving smoothing (EPS) method (AlBinHassan et al., 2006) to minimize the disturbance on ELPFs and derive the spectrum attenuation trend. The basic principle of the 1D EPS method can be described as follows. Given a L sample seismic trace, let X_j be the amplitude of the jth sample. For an N-point ($N < L$) 1D EPS, we first calculate the standard deviations for N shifted windows around target point X_j:

$$\begin{aligned}&\text{window 1}: \quad \left(X_{j-N+1},\ldots,X_{j-1},X_j\right),\\ &\text{window 2}: \quad \left(X_{j-N+2},\ldots,X_j,X_{j+1}\right),\\ &\qquad\qquad\vdots\\ &\text{window N}: \quad \left(X_j,X_{j+1},\ldots,X_{j+N-1}\right),\end{aligned}$$

let I_i be the collection of indexes of the points in the ith window, and calculate the standard deviation for window i as

$$d_i = \left[\frac{1}{N}\sum_{n\in I_i}\left(X_j - X_n\right)^2\right]^{1/2}. \tag{6}$$

Then we can obtain a set of standard deviations $\{d_1, d_2 \ldots, d_N\}$. The window that has the minimum standard deviation is selected, and its average value is assigned as the output at the jth output location. Repeating this process for every location will yield the final output. Fig. 6 uses a step function (Fig. 6a) to illustrate the idea of 1D EPS. White Gaussian noise is added to the function (Fig. 6b). Fig. 6c is obtained by applying a 21-point moving average smoothing filter to the noisy step function. The noise is obviously reduced, but the sharp edge of the input step function is still blurred. In contrast, applying a 21-point 1D

Table 1
Algorithm for spectrum attenuation selection.

Input: EPS smoothed ELPFs located at the local peaks of seismic envelope, hereafter termed EPS_ELPFs(envelope)
Output: Spectrum attenuation selector. If spectrum attenuation is related to hydrocarbon selector = 1, else selector = 0.
1. set **selector (t) = 0**;
2. find f_{ps1}, t_{ps1_b}, and t_{ps1_e};
3. find f_{ps2}, t_{ps2_b}, and t_{ps2_e};
4. set $f_{p0} = f_{ps1}$, $\Delta t = t_{ps2\_b} - t_{ps1\_e}$, Q = 50, calculate f_p by Eq. (7),
If $f_{ps2} \le f_p$, **selector**(t_{ps1_e} to t_{ps2_e}) **= 1**;
5. delete EPS_ELPFs(envelope) before t_{ps1_e};
6. if $t_N > t_{ps2\_e}$, let $f_{ps1} = f_{ps2}$, $t_{ps1\_b} = t_{ps2\_b}$, $t_{ps1\_e} = t_{ps2\_e}$, go to 3.

Table 2
Some interpretations of the selection algorithm.

t_N	location of the last point of EPS_ELPFs(envelope)
f_{ps1}	the maximum value of EPS_ELPFs(envelope)
t_{ps1_b}	location of the first point of EPS_ELPFs(envelope) equaling to f_{ps1}
t_{ps1_e}	location of the last point of EPS_ELPFs(envelope) equaling to f_{ps1}
f_{ps2}	the second maximum value of EPS_ELPFs(envelope)
t_{ps2_b}	location of the first point of EPS_ELPFs(envelope) equaling to f_{ps2}
t_{ps2_e}	location of the last point of EPS_ELPFs(envelope) equaling to f_{ps2}
f_{p0}	initial peak frequency of Ricker wavelet in Eq. (7)
f_p	after a time interval Δt, the peak frequency of Ricker wavelet

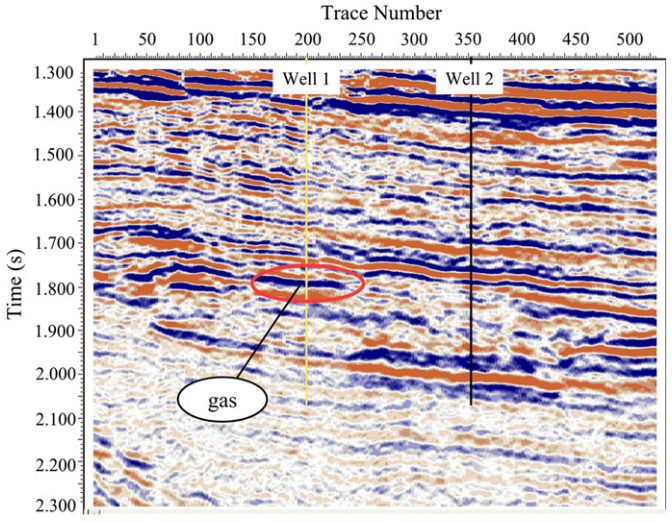

Fig. 7. A seismic section from the original seismic data volume. Well 1 produces gas around 1.800 s, as indicated by the ellipse. Well 2 doesn't produce hydrocarbon in this section.

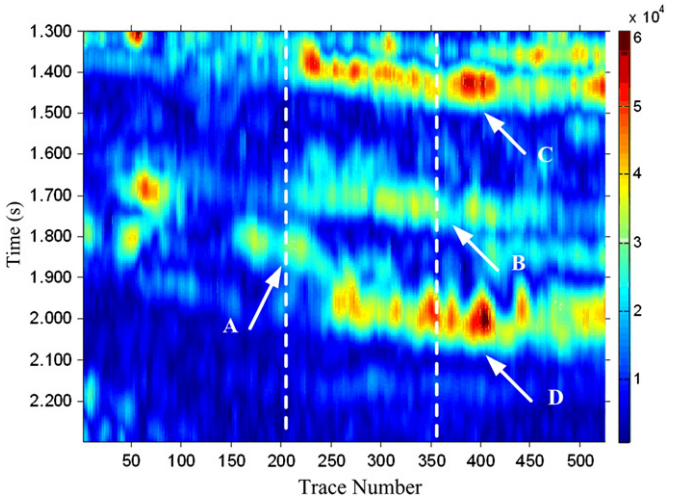

Fig. 8. Low frequency energy (5–15 Hz) of Fig. 7 calculated by Eq. (4).

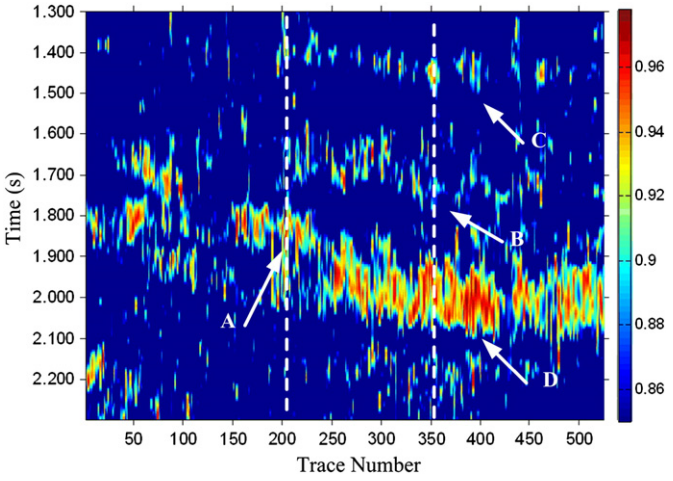

Fig. 10. Spectrum attenuation calculated by Eq. (5) with low frequency in 5–15 Hz and high frequency in 70–80 Hz of Fig. 7. For easier recognition, this figure only displays amplitude larger than 0.85.

EPS filter (Fig. 6d) preserves the sharp change while successfully reducing noise. Thus, this smoothing method can group the analysis point and its most homogenous surrounding neighboring samples together while preserving the sharp changes. Hence, we use this method to classify the equivalent local peak frequency located at the local peaks of seismic envelope to determine the spectrum attenuation trend, which will be illustrated in Figs. 11 and 12 in Section 3.

As we know, seismic attenuation is usually measured by a dimensionless quality (Q) factor. Following Waters (1978), Q is 5–50 for gas sandstone, 20–150 for sedimentary rock, and 75–150 for volcanic rock. The smaller the Q, the bigger the attenuation. So in this paper we take Q = 50 as the standard to determine whether the attenuation trend is associated with hydrocarbon. According to Zhang and Ulrych (2009), for a Ricker spectrum with its peak frequency being f_{p0} at time $t - \Delta t$, after a time interval Δt, the peak frequency at time t is

$$f_p = f_{p0}\left[\sqrt{\left(\frac{f_{p0}\pi\Delta t}{4Q}\right)^2 + 1} - \frac{f_{p0}\pi\Delta t}{4Q}\right]. \quad (7)$$

Therefore, we use the change of peak frequency of the Ricker wavelet with Q = 50 as the reference to determine whether the spectrum attenuation is really related to hydrocarbon. The spectrum attenuation selection algorithm is illustrated in Table 1 and the interpretations of the selection algorithm are addressed in Table 2.

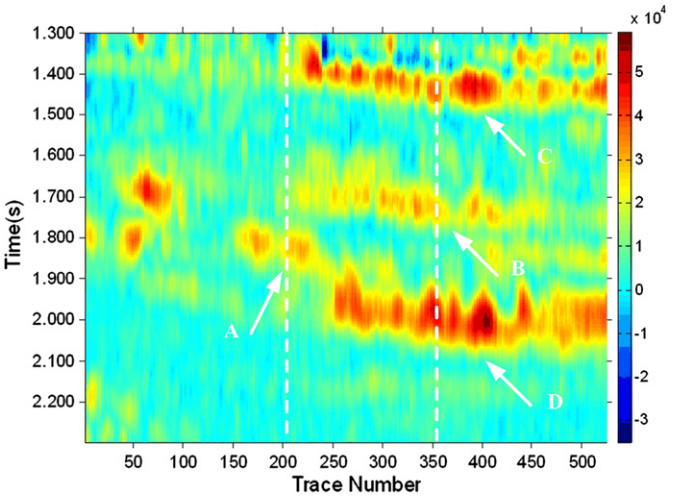

Fig. 9. Difference between the low frequency energy (5–15 Hz) calculated by Eq. (4) and high frequency energy (70–80 Hz) calculated by Eq. (3) of Fig. 7.

3. Data example

To confirm the effectiveness of the proposed method, we apply it to one section of a real seismic data volume from CNOOC. Fig. 7 shows a vertical seismic section through two wells extracted from a 3D volume. Well 1 produces gas at about 1800 ms, while Well 2 doesn't produce any hydrocarbon in this section. Fig. 8 shows the low frequency energy (5–15 Hz) profile of Fig. 7 obtained by Eq. (4). Fig. 9 shows the difference between the low frequency energy in Fig. 8 and the high frequency energy (70–80 Hz) obtained by Eq. (3). Fig. 10 is the spectrum attenuation calculated by Eq. (5). We found that Figs. 8 and 9 look similar, and they both contain the effect of strong reflection of the seismic section in Fig. 7, indicated by arrows B, C and D. In addition, in Figs. 8 and 9, the strong amplitude area indicated by arrows A is a gas reservoir, and it has the same amplitude intensity with the area indicated by arrows B. So it is easy to misinterpret the area indicated by arrows B as gas reservoir indicator. In Fig. 10, because we use the ratio to calculate the spectrum attenuation, the impact of strong reflection can be removed effectively, see the area indicated by arrows B and C. However, the area indicated by arrows D still contradicts the true result because of the interference.

In order to further improve the accuracy of hydrocarbon detection, we select the spectrum attenuation in Fig. 10 to remove disturbance caused by interference. Figs. 11 and 12 show the principle of constructing selector, taking Trace 200 around Well 1 and Trace 350 around Well 2 as examples respectively. To the 1D EPS method, short window is suitable for detecting small change, but it may be too sensitive to noises; while long window is good for detecting large change and is stable in noisy conditions, but it may lose the resolution. In practice, we can choose a balanced window length based on some prior information. In Figs. 11d and 12d, we use 5-point 1D EPS to repeatedly smooth ELPFs located at the local peaks of the envelope (green star) to obtain the smoothed ELPFs (red circle). In Fig. 11d, point P1 is at 1.7380 s, with peak frequency being 38.5856 Hz, point P2 is at 2.2280 s, and its peak frequency is 24.4000 Hz. Let f_{p0} = 38.5856 Hz, following Eq. (7), we obtain f_p = 28.7918 Hz, which is larger than 24.4000 Hz, so the spectrum attenuation in this section is corresponding to hydrocarbon. In Fig. 12d, point P1 is at 1.7640 s, with peak frequency at 25.76 Hz, point P2 is at 2.1620 s, with peak frequency at 24.80 Hz. Let f_{p0} = 25.76 Hz, following Eq. (7), we obtain f_p = 21.9434 Hz, which is smaller

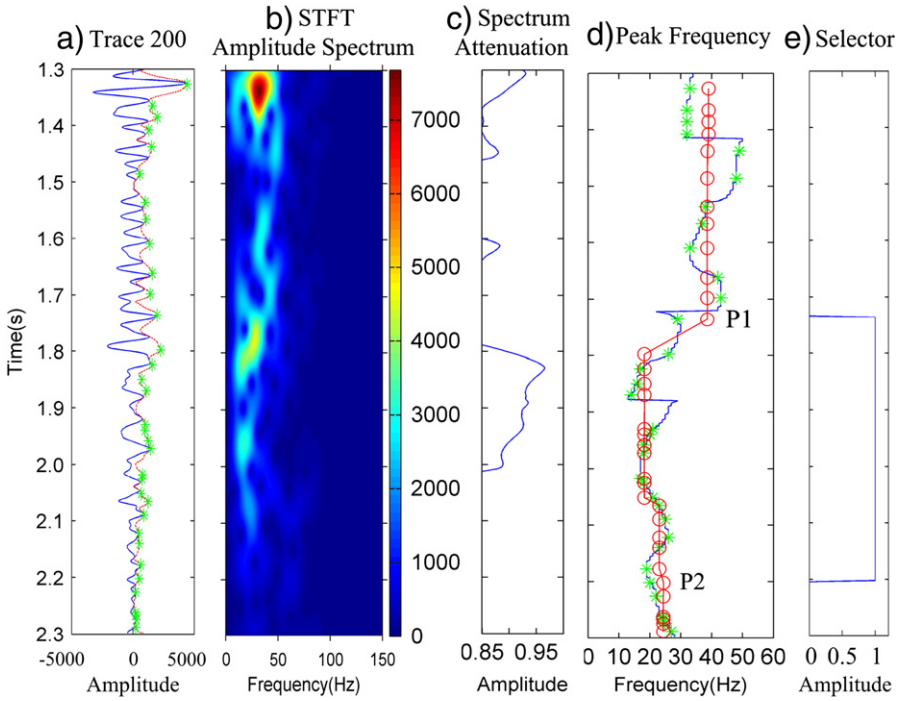

Fig. 11. (a) The 200th trace of the seismic section in Fig. 7 (blue solid line) with its envelope (red dashed line) and envelope peaks (green star); (b) The STFT amplitude spectrum of the trace in (a); (c) The spectrum attenuation, i.e. the 200th trace of Fig. 10; (d) The equivalent peak frequency (ELPF) of (b) (blue solid line), the ELPF located at envelope peaks (green star) and its corresponding smoothed ELPF (red circle); (e) The spectrum attenuation selector.

than 24.80 Hz, so the spectrum attenuation in this section is not corresponding to hydrocarbon. Fig. 13 shows the selectors of all traces in Fig. 7. Fig. 14 shows the selected spectrum attenuation obtained by multiplying the spectrum attenuation in Fig. 10 and the selectors in Fig. 13. It is shown that the selected spectrum attenuation can locate the hydrocarbon more precisely.

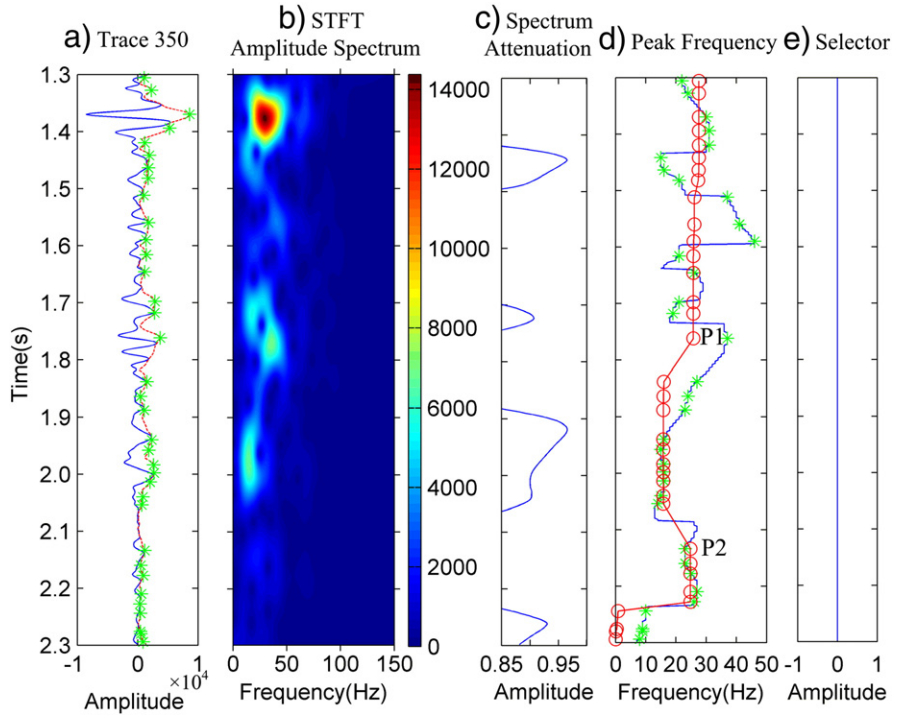

Fig. 12. (a) The 350th trace of the seismic section in Fig. 7 (blue solid line) with its envelope (red dashed line) and envelope peaks (green star); (b) The STFT amplitude spectrum of the trace in (a); (c) The spectrum attenuation, i.e. the 350th trace of Fig. 10; (d) The ELPF of (b) (blue solid line), the ELPF located at envelope peaks (green star) and its corresponding smoothed ELPF (red circle); (e) The spectrum attenuation selector.

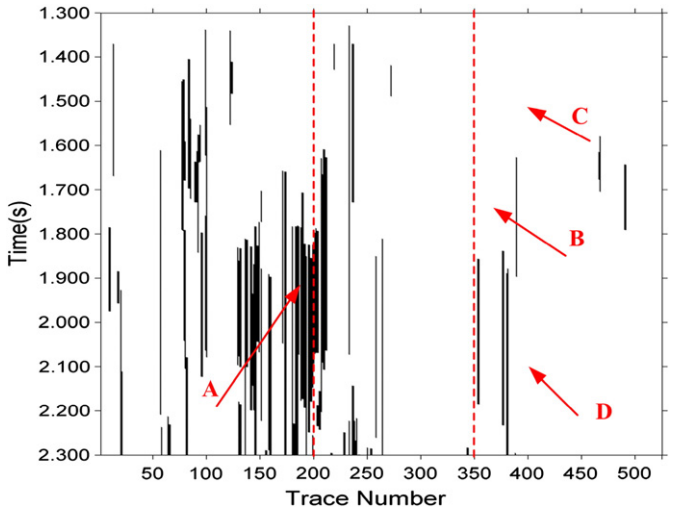

Fig. 13. Selectors of all traces in Fig. 7, where black is 1, white is 0.

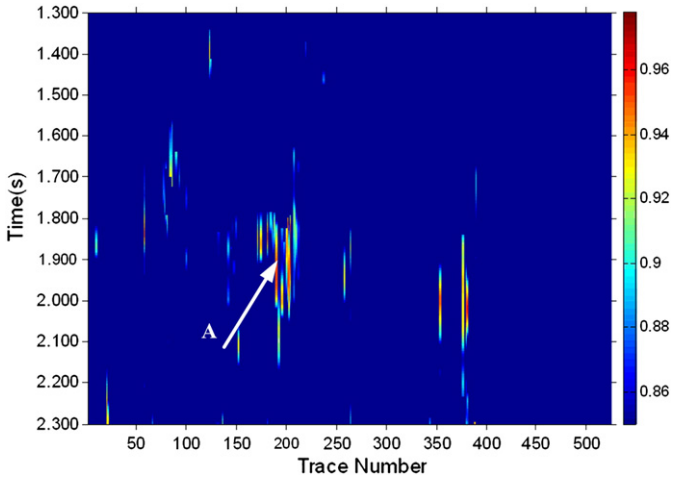

Fig. 14. The selected spectrum attenuation obtained by multiplying the spectrum attenuation in Fig. 10 and the selectors in Fig. 13.

4. Conclusions

In this paper, we have shown that hydrocarbon detection using adaptively selected spectrum attenuation is more accurate than that of using high frequency attenuation anomalies, and/or low frequency information directly. The spectrum attenuation is calculated by the ratio of high frequency components to low frequency components, so it combines both the high and low frequency information, this can avoid the impact of strong amplitude anomaly. The spectrum attenuation is adaptively selected based on the spectrum attenuation trend which is measured by the change of EPS smoothed ELPFs located at the local peaks of the envelope by taking the variation of the peak frequency of Ricker wavelet with Q = 50 as the reference. So the selected spectrum attenuation can remove disturbance caused by interference. A real seismic data example demonstrates the validity of our method.

It is noted that the seismic attenuation trend can be measured using ELPFs based on STFT. In practice, after obtaining spectrum attenuation, it often may not be necessary to compute spectrum attenuation selector for every trace. We only need to compute it for several sampled traces among potential hydrocarbon area to confirm reservoir. Besides, we also can combine the spectrum attenuation selection method proposed in Section 2.3 with other similar spectrum attenuation methods, such as ISA (Castagna et al., 2003), to minimize the influence of interference and get more reliable result. However, due to the influence of interference and noises etc., we may not exactly extract the equivalent wavelet of each segment from STFT amplitude spectrum by a smoothing method. Although the influence is reduced by the edge-preserving smoothing (EPS) method, we may use multiple traces to further reduce the influence, which may need further investigation.

Acknowledgments

We would like to thank the CNOOC Research Center for providing the data and support, and the China Postdoctoral Science Foundation (2013M532028), National Natural Science Foundation of China (41390454; 91330204), Important National Science & Technology Specific Projects of China (2011ZX05023005) for funding this work.

References

AlBinHassan, N.M., Luo, Y., Al-Faraj, M.N., 2006. 3D edge-preserving smoothing and applications. Geophysics 71 (4), 5–11 (July–August).
Biot, M.A., 1956. Theory of propagation of elastic waves in a fluid-saturated porous solid, 1. Low-frequency range. J. Acoust. Soc. Am. 28 (2), 168–178.
Castagna, J.P., Sun, S.J., Siegfried, R.W., 2003. Instantaneous spectral analysis: detection of low-frequency shadows associated with hydrocarbons. Lead. Edge 22 (2), 120–127.
Chen, W.C., Gao, J.H., 2007. Characteristic analysis of seismic attenuation using MBMSW wavelets. Chin. J. Geophys. 50 (3), 837–843 (in Chinese).
Ebrom, Dan, 2004. The low-frequency gas shadow on seismic sections. Lead. Edge 23 (8), 772.
Goloshubin, G.M., Korneev, V.A., 2000. Seismic low-frequency effects from fluid-saturated reservoir. Expanded Abstracts of 70th SEG Ann Internat Mtg, pp. 1671–1674.
Hu, X.P., Chen, Y.J., Liang, X.W., Lang, K.R., 2005. New technology for direct hydrocarbon reservoir detection using seismic information. 75th Annual International Meeting, SEG, Expanded Abstracts, pp. 1735–1738.
Hu, X.P., Liang, Y., Tao, C.F., Liu, X.B., Lang, K.R., 2009. Application of hydrocarbon detection technology based on double-phase medium theory. Expanded Abstracts of 79th Annual International Meeting, SEG, pp. 593–597.
Jiang, L., Yang, S.G., Zhao, M.J., Yang, S.N., 2010. Frequency-dependent seismic attributes and their application for hydrocarbon detection. 80th Annual International Meeting, SEG, Expanded Abstracts, pp. 1566–1570.
Klimentos, T., 1995. Attenuation of P- and S-waves as a method of distinguishing gas and condensate from oil and water. Geophysics 60 (2), 447–458.
Korneev, V.A., Goloshubin, G.M., Daley, T.M., Silin, D.B., 2004. Seismic low frequency effects in monitoring fluid-saturated reservoirs. Geophysics 69 (2), 522–532.
Mallat, S., 2003. A Wavelet Tour of Signal Processing, Second edition. Elsevier Pte Ltd., Singapore.
Mitchell, J.T., Derzhi, N., Lichma, E., 1996. Energy absorption analysis: a case study. Expanded Abstracts of 66th Annual International Meeting, SEG, pp. 1785–1788.
Palmer, I.D., Traviolia, M.L., 1980. Attenuation by squirt flow in undersaturated gas sands. Geophysics 45 (12), 1780–1792.
Sa, L.M., Wang, S.X., Mu, Y.G., Liang, X.W., Liu, Quanxin, 2004. A new method for hydrocarbon detection based on multi-phase theory. Appl. Geophys. 1 (2), 83–88.
Waters, K.H., 1978. Reflection Seismology. Wiley, New York.
Zhang, C.J., Ulrych, T.J., 2002. Estimation of quality factors from CMP records. Geophysics 67 (5), 1542–1547.
Zhang, C.J., Ulrych, T.J., 2009. Reflectivity guided Q analysis for reservoir description. Expanded Abstracts of 79th Annual International Meeting, SEG, pp. 2332–2335.
Zhou, D.H., Fu, Zh.F., An, P., 2010. Case studies on hydrocarbon prediction using wavelet-based spectrum and spectrum attenuation approach. Expanded Abstracts of 80th Annual International Meeting, SEG, pp. 2386–2390.